ARTICLE

Double Stimuli-Responsive Ultrafiltration Membranes from Polystyrene-*block*-poly(*N*,*N*-dimethylaminoethyl methacrylate) Diblock Copolymers

Felix Schacher,*,† Tobias Rudolph,† Florian Wieberger,‡ Mathias Ulbricht,§ and Axel H. E. Müller*,†

Makromolekulare Chemie II and Makromolekulare Chemie I, Universität Bayreuth, Universitässtrasse 30, D-95440 Bayreuth, and Technische Chemie II, Universität Duisburg-Essen, Universitätsstrasse 2, D-45117 Essen

ABSTRACT We report on the formation of self-supporting, double stimuli-responsive ultrafiltration membranes via the non-solvent-induced phase separation (NIPS) process. The polymers, polystyrene-*block*-poly(*N*,*N*-dimethylaminoethyl methacrylate) (PS-*b*-PDMAEMA), were synthesized via living anionic polymerization in THF using *sec*-butyllithium as initiator. Two amphiphilic diblock copolymers were used, $S_{81}D_{19}^{75}$ and $S_{68}D_{32}^{100}$. The membranes were cast from mixtures of THF and DMF. The influence of the solvent composition, the "open-time" before immersion into the coagulation bath, and the casting film thickness onto the membrane morphology were thoroughly investigated, and flux values obtained for the different membrane systems were compared. The higher content in hydrophilic polymer for $S_{68}D_{32}^{100}$ resulted in a better compatibility with the nonsolvent bath consisting of water, leading to a slower precipitation and thus an improved control of the phase separation occurring. Under certain conditions, ordered microphase-separated porous morphologies were observed in parts of the membrane cross-section. Further, the "smart" properties of those novel materials are shown for two representative systems. It could be demonstrated that both stimuli for PDMAEMA, pH and temperature, can be reversibly and independently applied in order to significantly change the transmembrane water flux.

KEYWORDS: Membranes • polymeric materials • assembly • porous materials • block copolymers

INTRODUCTION

In the past decade, membrane separations have gained high technical relevance in a wide range of applications, from water purification to medical applications (1). Increasing complexity in modern separation processes is accompanied by demanding and further specialized requirements for a suitable membrane, by far exceeding commonly known properties like chemical inertness, thermal and mechanical stability, and mechanical strength. Especially when it comes to new technically challenging or commercially attractive separation problems, many state-of-the-art membranes are facing their limitations.

Polymers are by far the most important membrane materials, especially because of the relative ease and flexibility of manufacturing a large diversity of effective barrier structures for different membrane processes. Possible pathways toward the design of novel membranes are the modification of already-established membrane structures, an alteration of the preparation techniques, or the use of new building blocks with improved functionalities. Furthermore, attempts have been made to blend hydrophobic and hydrophilic compounds, mainly focusing on the improvement of both fouling characteristics and membrane morphology (2). The activities in this field have been reviewed recently (3). Main challenges for the development of novel ultrafiltration membranes are a narrow and adjustable pore size distribution and a thin barrier layer so that the trade-off between high selectivity and high flux could be overcome (4). In addition, the fouling tendency should be minimized.

Using block copolymers as building blocks represents a facile and straightforward methodology for the simple incorporation of different structural or chemical features into bulk materials. Junctions between two compartments are covalent and therefore thermodynamically, chemically, and mechanically stable (5, 6). Especially amphiphilic block copolymers have received considerable interest concerning their synthesis via living (7) or controlled polymerization techniques (8) and their self-assembly in the bulk (9−11), in thin-films (12), or in solution (13). Through recent advances, block copolymer dimensions on the nanoscale and resulting morphologies become more and more predictable. In that way, block copolymers are able to combine the superior mechanical properties of hydrophobic and the wettability and surface chemistry of hydrophilic materials. Moreover, smart polymeric materials render these structures sensitive to external stimuli like pH (14), temperature (15), or light (16) and broaden the scope of possible applications of such systems. First attempts had been made to prepare

* Corresponding author. E-mail: axel.mueller@uni-bayreuth.de (A.H.E.M.); felix.schacher@uni-bayreuth.de (F.S.).
Received for review March 16, 2009 and accepted May 31, 2009
† Makromolekulare Chemie II, Universität Bayreuth.
‡ Makromolekulare Chemie I, Universität Bayreuth.
§ Universität Duisburg-Essen.
DOI: 10.1021/am900175u

Published on Web 06/17/2009

ultrafiltration membranes from diblock copolymers by using one block as pore template: after film formation, an annealing step was crucial to obtain well-defined microphase-separated morphologies in the bulk of the polymer film, and then a selective dissolution or etching step had to be performed (17, 18).

One of the most important industrial processes for the fabrication of integrally anisotropic ("asymmetric") polymer membranes is non-solvent-induced phase separation (NIPS), where a casted film of a polymer solution is immersed in a precipitation bath (19). This is a straightforward and fast one-step procedure. Membrane morphology and barrier structure can be controlled by a range of parameters; most important are the mutual interactions between membrane polymer and solvent (or solvent mixture) on the one hand, and between polymer and nonsolvent on the other hand (polymer solvent and nonsolvent must be miscible). In addition to the thermodynamic boundary conditions, the kinetics of mass transfer and phase separation can have a decisive influence (20). The obtained materials typically exhibit a very thin "skin" layer, which strongly determines the separation properties and is mechanically supported by a macroporous substructure (20). Such "asymmetric" membranes find their applications in pressure-driven separation processes such as ultrafiltration, nanofiltration, or reverse osmosis. If water is used as nonsolvent, phase separation of amphiphilic block copolymers should result in a hydrophobic matrix featuring pores which are coated with the hydrophilic compartment. Recently, this has been demonstrated for well-defined block copolymers, polystyrene-*block*-poly(4-vinylpyridine) (21). Here, poly(4-vinylpyridine) should cover the pore interior and serve as a weak polyelectrolyte, rendering the membranes pH-sensitive; however, this had not been studied. Other attempts toward stimuli-responsive membranes via immersion precipitation are based on statistical (22) or grafted (23) block copolymers with smart properties. In our groups, a well-defined polystyrene-*block*-poly(*N,N*-dimethylaminoethyl methacrylate) (PS-*b*-PDMAEMA) block copolymer was shown to form self-supporting asymmetric membranes via the NIPS process from solvent mixtures of THF and DMF (24). This polymer, $S_{81}D_{19}^{75}$, was synthesized via sequential anionic polymerization techniques (7). Note that the subscripts correspond to the weight fractions of the corresponding blocks and the superscript is the absolute molecular weight in kg/mol. We could show that these membranes are able to react onto two independently addressable stimuli, pH and temperature, in terms of water flux and effective pore size, attributed to the smart properties of the hydrophilic block, PDMAEMA (15).

Within this contribution, we considerably extend our earlier work. A block copolymer comprising a higher content of hydrophilic material, $S_{68}D_{32}^{100}$, was synthesized in an analogous way and also used for the fabrication of stimuli-responsive asymmetric membranes. The parameters of the membrane casting process, NIPS, were systemically varied for both $S_{81}D_{19}^{75}$ and $S_{68}D_{32}^{100}$. First, the influence of the composition of the solvent mixture (THF and DMF) for the casting solution on the resulting membrane morphology and performance is thoroughly investigated. Further, the influences of different "open times" in between film casting and the immersion into the coagulation bath as well as of varied casted film thickness were studied. All obtained membrane structures were analyzed with scanning electron microscopic techniques, and the corresponding water fluxes were determined. Finally, the double stimuli-responsive character for one representative membrane of each polymer is demonstrated through pH- and temperature-dependent flux measurements. Although not all parameters that could have influence on membrane structure for the presented system consisting of block copolymer, THF, DMF, and water are exhaustively addressed, we are able to point out important tendencies, and the results can be interpreted in a conclusive way. Please note that we are dealing with a combination of two ternary phase diagrams, polymer, solvent, and nonsolvent for each of the two blocks, providing a complex multiparameter space.

EXPERIMENTAL SECTION

Materials. *sec*-Butyllithium (Acros) was used as delivered. THF (Fluka) was distilled from CaH_2 and K, subsequently. Afterward, the solvent was directly transferred into the stirred glass reactor. Styrene was kindly provided by BASF and was stirred over Bu_2Mg (Aldrich) and afterward condensed on a vacuum line into glass ampoules. *N,N*-Dimethylaminoethyl methacrylate (Aldrich) was stirred with trioctylaluminium (Aldrich) and afterward condensed on a vacuum line. 1,1-Diphenylethylene (Aldrich) was distilled from *sec*-butyllithium and stored under nitrogen.

Synthesis. Polystyrene-*block*-poly(*N,N*-dimethylaminoethyl methacrylate) was synthesized via sequential living anionic polymerization in THF (500 mL) at low temperatures in the presence of alkoxides to stabilize the living chain end. The detailed procedure has already been described (7). For $S_{68}D_{32}^{100}$, first styrene (68 g, 0.65 mol) was initiated with *sec*-butyllithium (1.3 mL, 0.99 mmol) at −70 °C. Afterward, the reaction was allowed to proceed at −70 °C for 30 min. For polymerization of the second block, the polystyrene chains were end-capped with 1,1-diphenylethylene (0.36 mL, 2 mmol) at −50 °C in order to attenuate the reactivity of the anions (25, 26). Otherwise, attack of the ester moiety would occur upon addition of *N,N*-dimethylaminoethyl methacrylate. The latter (32 g, 0.21 mol) was injected via syringe into the reaction vessel and was polymerized for 1 h at −40 °C. Finally, the reaction was stopped through addition of 3 mL of degassed isopropanol, and the polymer was purified through dialysis against THF and dioxane and freeze-dried. $S_{81}D_{19}^{75}$ has been prepared in an analogous way, employing both monomers in the appropriate ratio.

Membrane Preparation. Membranes were prepared via the NIPS process. Films were cast from a solution of PS-*b*-PDMAEMA (1.5 g, 15 wt %), and a mixture of DMF and THF with a doctor blade onto polished glass substrates. After the so-called "open time" in contact with air (relative humidity was 30−40 % and temperature was ∼20 °C), the as-cast films were immersed into a bath containing deionized water for final formation of the membrane morphology. During the next 60 min, the films started to lift off the glass surface. After 12 h, the membranes were taken out of the water bath and stored in deionized water until they were used for water flux measurements.

Water Flux Measurements. Water flux measurements were carried out in a stirred ultrafiltration test cell (Amicon 8010, Millipore, effective membrane diameter 22 mm) connected to a water reservoir at a constant water column height of 25 cm,

Table 1. Water Flux for Different Solvent Compositions and Different "Open Times"

Water Flux for Different Solvent Compositions					
solvent composition (% THF/% DMF)	25/75	40/60	50/50	60/40	75/25
Water flux for $S_{81}D_{19}^{75}$ [L/(m^2 h bar)]	200	4400	2500	4100	1400
water flux for $S_{68}D_{32}^{100}$ [L/(m^2 h bar)]	100	70	100	2100	150

Water Flux for Different "Open Times"						
"open time"	0	30 s	60 s	90 s	2 min	10 min
water flux for $S_{81}D_{19}^{75}$ [L/(m^2 h bar)]	0	4800	4100	0	[a]	[a]
water flux for $S_{68}D_{32}^{100}$ [L/(m^2 h bar)]	0	[b]	2100	[b]	100	100

[a] Not determined; no structural change observed for "open times" exceeding 90 s. [b] Not determined; no membrane was prepared under these conditions.

providing a transmembrane pressure of 0.025 bar. Values provided in Table 1 were obtained through averaging the obtained water fluxes for three membranes. Deviations in between membranes of the same cast film were in the range of 15%. The membrane was placed in this cell, which was immersed in a water bath kept at constant temperature. pH was adjusted through dilute solutions of NaOH and HCl in deionized water; after each change in pH, a time span of 2 h under flow-through was used to allow equilibration. Temperature ramps were performed through keeping the whole ultrafiltration cell in a tempered water bath. Steps were 10 °C, equilibration time in between two points was 1 h, except for the highest temperature (65 °C: 2 h).

Characterization. ***NMR.*** ^{1}H NMR measurements were performed on a Bruker 250 MHz AC spectrometer in $CDCl_3$ as solvent. The block copolymer composition was determined through the integral ratio between the styrene protons (5H, $\delta = 6.3-7.2$) and the CH_2 protons adjacent to the ester group group of DMAEMA (2H, $\delta = 4.1$).

Size Exclusion Chromatography. Size exclusion chromatography (SEC) measurements were performed on a set of 30 cm SDV-gel columns of 5 mm particle size having a pore size of 1×10^5, 1×10^4, 1×10^3 and 1×10^2 Å with refractive index and UV ($\lambda = 254$ nm) detection. SEC was measured at an elution rate of 1 mL/min with THF containing 0.25 wt % tetra-butylammoniumbromide (TBAB) as eluent.

Scanning Electron Microscopy. SEM was carried out on a Leo Gemini 1530. The specimens were dried under vacuum overnight and coated with approximately 2 nm Pd. For the cross-sections, a piece of the sample was frozen together with the sample holder and broken afterward.

Transmission Electron Microscopy. TEM micrographs were taken on a Zeiss CEM 902 operating at 80 kV.

Dynamic Light Scattering. Dynamic light scattering (DLS) measurements were performed in sealed cylindrical scattering cells ($d = 10$ mm) at a scattering angle of 90° on an ALV DLS/SLS-SP 5022F equipment consisting of an ALV-SP 125 laser goniometer with an ALV 5000/E correlator and a He−Ne laser with the wavelength $\lambda = 632.8$ nm. The CONTIN algorithm was applied to analyze the obtained correlation functions. Apparent hydrodynamic radii were calculated according to the Stokes−Einstein equation.

RESULTS AND DISCUSSION

Synthesis of the PS-*b*-PDMAEMA Block Copolymers. Two amphiphilic block copolymers were synthesized via sequential anionic polymerization in THF. After purification, they were characterized through a combination of ^{1}H NMR and SEC. The final composition was determined to be $S_{81}D_{19}^{75}$ and $S_{68}D_{32}^{100}$. Note that the subscripts refer to the weight fraction of the corresponding block and the superscript to the absolute molecular weight in kg/mol. The degrees of polymerization were $S_{600}D_{90}$ ($S_{81}D_{19}^{75}$) and $S_{650}D_{205}$ ($S_{68}D_{32}^{100}$). Both polymers exhibited a very narrow molecular weight distribution (polydispersity index (PDI) = 1.03 for $S_{81}D_{19}^{75}$ and 1.08 for $S_{68}D_{32}^{100}$). The SEC traces with THF and additional 0.25% TBAB as eluent and the ^{1}H NMR spectrum for $S_{68}D_{32}^{100}$ are shown in Figure 1.

During the polymerization of $S_{68}D_{32}^{100}$, a small amount of recombination occurred, as visible in the SEC trace in Figure 1A. That also explains the slightly increased PDI. The molecular weight of the first block, polystyrene, was determined with a PS calibration curve. The NMR in Figure 1B was used to determine the length of the second block, PDMAEMA, via the comparison of the styrenic protons (a, 5H, $\delta = 6.2-7.3$) and the methylene group of DMAEMA adjacent to the ester moiety (e, 2H, $\delta = 4.1$). The contribution from the single 1,1-diphenylethylene used for end-capping of the living PS chains for the NMR integral of the PS protons was negligible.

Membrane Preparation and Characterization. All membranes were prepared via the NIPS process. Mixtures of THF and DMF that are supposed to mix ideally and are both miscible with water in the coagulation bath were selected as solvent for the block copolymers. THF is supposed to be the better solvent for PS, DMF for PDMAEMA. Polymer solutions of 15 wt % in THF/DMF mixtures were cast on a precleaned planar glass substrate using a doctor blade with different step heights (50−200 μm). After film-casting, the solvent was allowed to evaporate for a certain amount of time (up to 10 min) before the whole substrate was immersed into the nonsolvent bath. This is the so-called "open time". During this step, mostly the higher volatile solvent (here THF) evaporates; the polymer enriches at the polymer−air interface and eventually phase separation could even start in the top layer of the "proto-membrane". We suppose that this step is crucial for the formation of the pores of the separation layer as well as the overall porous membrane structure. After immersion in the precipitation bath, final solvent exchange and solid film formation took place.

In an earlier work, we had shown that for a mixture of THF (50%) and DMF (50%), a polymer concentration of 15 wt %, a doctor blade step height of 200 μm, an "open time" of 60 s, and deionized water as the coagulation bath, double

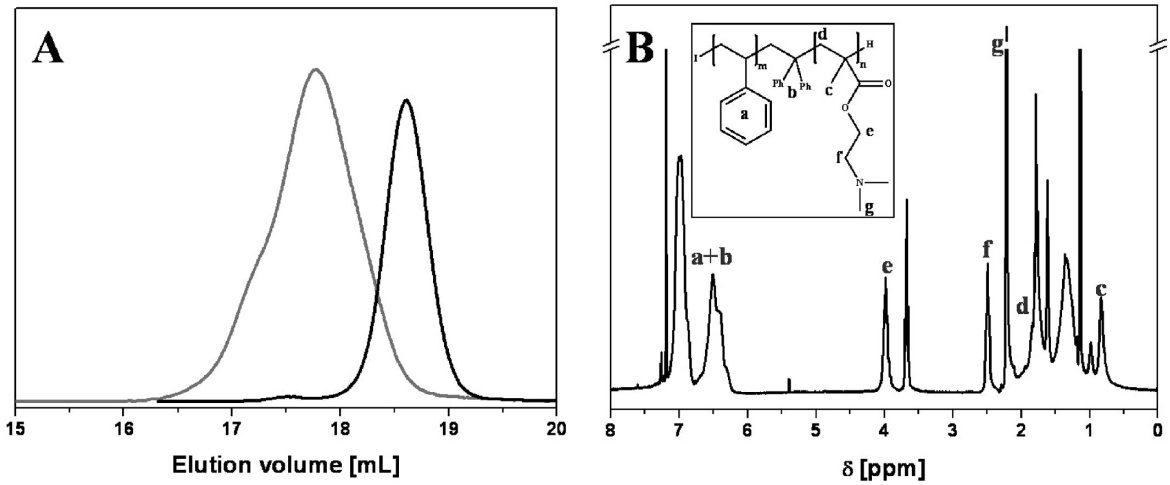

FIGURE 1. (A) SEC traces for the S^{68} precursor (solid black line) and $S_{68}D_{32}{}^{100}$ (solid gray line) with THF and additional 0.25 wt % TBAB as eluent; (B) ^{1}H NMR spectrum in $CDCl_3$ for $S_{68}D_{32}{}^{100}$, the inset shows the chemical structure of the AB diblock copolymer and the assignment of the important NMR signals.

stimuli-responsive membranes with addressable effective pore size could be obtained for $S_{81}D_{19}{}^{75}$ (24). These asymmetric membranes exhibited two independently addressable stimuli, pH and temperature, attributed to the smart properties of the second block, PDMAEMA. We now extend this work to another polymer, $S_{68}D_{32}{}^{100}$. The higher content of the second block, PDMAEMA, should have an influence on the membrane morphology under similar casting/NIPS conditions as the hydrophilic-to-hydrophobic balance of the diblock copolymer is altered. A higher content of DMAEMA should increase the compatibility with the coagulation bath and therefore result in a slower, more controlled precipitation or phase separation.

The aggregation behavior of PS-*b*-PDMAEMA in dilute aqueous solution under the same conditions was studied. Solutions with a polymer concentration of 1−5 g/L were prepared in a mixture of THF (50%) and DMF (50%), and the solvent was then exchanged against deionized water via dialysis. Both polymers formed spherical core−corona micelles in water at pH 6 with $\langle R_h \rangle_z = 35$ nm ($S_{81}D_{19}{}^{75}$, $DP_{DMAEMA} = 90$) and $\langle R_h \rangle_z = 45$ nm ($S_{68}D_{32}{}^{100}$, $DP_{DMAEMA} = 205$), as revealed via dynamic light scattering and transmission electron microscopic techniques (DLS and TEM results are not shown here). The size difference can be tentatively explained through the block length of the corresponding PDMAEMA compartment. Under these conditions, the polymer chains are protonated and moderately stretched. In both cases, the length of the PS block is comparable. The details of the phase diagram of such block copolymers in the bulk are not known, but according to their composition and volume fractions, the equilibrated materials should form cylindrical morphologies. We estimated the χ-parameter for this system by using the solubility parameters for PS (9.1 $(cal/cm^3)^{1/2}$) and PDMAEMA (9.21 $(cal/cm^3)^{1/2}$) (27). This resulted in a value of 0.024, which is rather small. If the corresponding degrees of polymerization are used (600 + 90 for $S_{81}D_{19}{}^{75}$ and 650 + 205 for $S_{68}D_{32}{}^{100}$), χN has a value of 16.8 and 20.5, indicating phase separation of the two blocks taking place. One may, of course, speculate about the applicability of this method for a system where the solubility parameters are rather close.

In the following, first a detailed description of one representative membrane structure is given. Thereafter, the influences of solvent composition, "open time", and casted film thickness are discussed in separate sections.

Asymmetric Membrane Structure. The NIPS process typically generates membranes with an anisotropic cross-section. We obtained this for several combinations of the varied parameters. Exemplarily, the structure obtained for a mixture of THF (60%) and DMF (40%), an "open time" of 60 s, and a casted film thickness of 200 μm is shown in Figure 2.

Figure 2A displays a cross-section of the membrane. The membrane thickness as determined via SEM was 80 ± 10 μm, and the anisotropic nature is evident. A thin separation layer with a thickness of around 1 μm and a compact spongelike structure was obtained at the surface formerly in contact with air (Figure 2B). Beneath the top layer, broader "fingerlike" channels appeared, the so-called "macrovoids". These develop during the immersion in the coagulation bath. Membrane structures like this are typical for systems which show "instantaneous demixing" during the NIPS process (20, 28). Here, the rapid precipitation upon contact with water was attributed to the PS part of the PS-*b*-PDMAEMA block copolymers. The anisotropy then results from both time delay and an uneven composition distribution throughout the whole film during the solvent/nonsolvent exchange. Macrovoids like obtained in this case are acceptable for "medium pressure" applications like ultra- or microfiltration. Figure 2C presents an on-top view onto the membrane surface. The structure is not well-ordered; no long-range order could be seen. The appearance was rather spongelike. Although the pore sizes obtained via SEM were in the range of 20−80 nm, the effective barrier pore size for a comparable structure was shown to be in the range of 15−30 nm (24). This would position the membrane at the borderline between ultra- and microfiltration (3). The bottom surface,

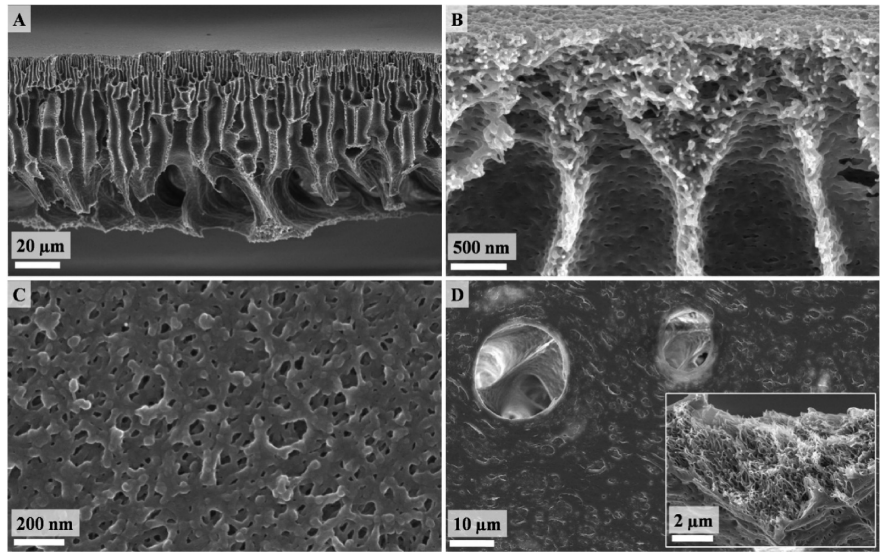

FIGURE 2. SEM micrographs of a $S_{81}D_{19}^{75}$ membrane prepared via the NIPS process (60% THF/40% DMF, 200 μm; 60 s); (A, B) cross-sections at different magnifications; (C) top view onto the membrane surface; (D) view onto the bottom of the membrane, the inset shows the structure obtained in the proximity of the bottom surface.

which has been in contact with the glass substrate, is shown in Figure 2D. Large pores with sizes up to 20 μm were present. All observed features of the membrane pore structure should yield high water fluxes. The inset in Figure 2D highlights the structure obtained in close proximity to the bottom of the membrane, e.g., on an edge originating from the cross-section preparation. Wormlike, interconnecting objects could be seen. Apparently, the time delay for demixing between top and bottom surface of the casted film lead to a more controlled phase separation and resulted in structural features that are different from those for precipitated standard membrane polymers. This will be discussed in more detail in the following sections.

Influence of the Solvent Composition. The choice of the polymer solvent is a crucial parameter for the NIPS process. Here, mixtures of THF and DMF were used, and the compositions varied from 25%/75% to 75%/25% for both $S_{81}D_{19}^{75}$ and $S_{68}D_{32}^{100}$. The two compartments, PS and PDMAEMA, are inherently different in their chemical nature. Although PDMAEMA is soluble in water, PS is completely insoluble. Further, THF is supposed to be the better solvent for PS, and DMF for PDMAEMA. As THF is more volatile than DMF, during the "open time", mostly THF evaporates in the top layer of the "proto-membrane". This, in combination with the hydrophobicity of the PS block, ensured immediate precipitation upon contact of the film with the coagulation bath. To investigate the effect of the solvent composition on the final membrane morphology and performance, we cast both $S_{81}D_{19}^{75}$ and $S_{68}D_{32}^{100}$ membranes from solutions of 75% THF/25% DMF, 60% THF/40% DMF, 50% THF/50% DMF, 40% THF/60% DMF, and 25% THF/75% DMF. In all cases, the "open time" was 60 s, and the casted film thickness was 200 μm. SEM micrographs for all prepared samples are shown in Figure 3. The insets in the SEM micrographs show enlargements of the cross-section (upper inset) and the membrane morphology on the bottom of the membrane (lower inset), if found different from that of the top section. The gray bars on the right-hand side of Figure 3 display the solvent composition used for the fabrication of the respective two membranes: dark gray corresponds to the THF, lighter gray to the DMF content.

First, the influence of the solvent composition will be described for each polymer separately. Afterward, both polymers will be compared. The left column shows the obtained structures for $S_{81}D_{19}^{75}$ (Figure 3A, C, E, G, I). At first glance, all the membranes exhibited similar morphologies. A thin, compact separation layer was formed on top of a macroporous support with "fingerlike" macrovoids oriented perpendicular to the glass substrate. The membrane thickness also was comparable in all cases and in the range of 80−90 μm, as determined via cross-sectional SEM. The upper inset in each micrograph presents an enlargement of the separation layer. Typically, this part had a thickness of around 1 μm, except for a casting solution of 40% THF/60% DMF (Figure 3C). Here the top layer was around 15−20 μm thick. Apart from that, both structure and porosity of the skin layer seemed to be independent from the solvent mixture used for film casting. Contrary, as shown in the lower inset in Figure 3C, at the bottom surface of the membrane wormlike structures were formed with a thickness of 60−70 nm and a length of up to several micrometers. In some cases, even interconnecting networks of such worms could be found. Obviously, the mechanism for the structure formation here strongly differs from that of the top layer. This may result from a different solvent composition present at the bottom of the polymer film following the immersion into the water bath. Surprisingly, such wormlike objects were not found for lower or for slightly higher THF contents of the casting solution (note that the membrane from 40% THF/60% DMF had also a different "skin" layer thickness). However, upon increasing the amount of THF to 75%, similar observations could be made (Figure 3I, lower inset). Here, the cylindrical aggregates seemed to be far more developed, visible through the even appearance of the sur-

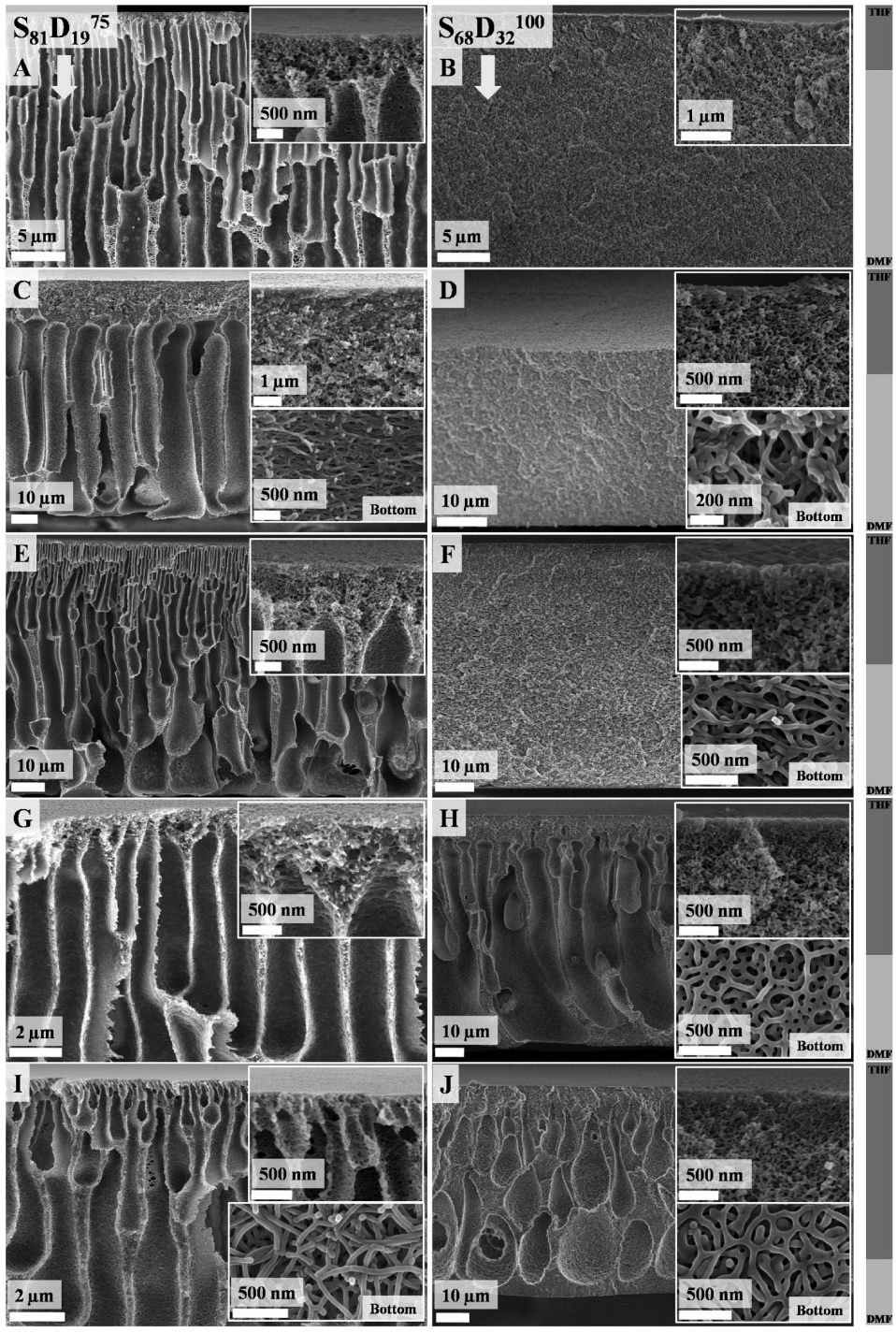

FIGURE 3. SEM micrographs for $S_{81}D_{19}^{75}$ and $S_{68}D_{32}^{100}$ membranes cast from different solvent mixtures: the left column shows $S_{81}D_{19}^{75}$, the right column $S_{68}D_{32}^{100}$, the gray bars to the right correspond to the solvent composition (dark gray, THF; lighter gray, DMF); the solvent composition was (A, B) 25% THF/75% DMF, (C, D) 40% THF/60% DMF, (E, F) 50% THF/50% DMF, (G, H) 60% THF/40% DMF, and (I, J) 75% THF/25% DMF; the corresponding insets show enlargements of the respective cross-section (upper inset) and the membrane morphology at the bottom of the structure (lower inset), if found to be different from the top layer.

face. They are better defined concerning the average diameter. Moreover, less junctions are formed, and the cylinders merely entangle.

The situation was different if the same experiments were carried out for the polymer with the higher content of hydrophilic material, $S_{68}D_{32}^{100}$ (Figure 3B, D, F, H, J). For the lowest content of THF (25%), the whole membrane cross-section exhibited a spongelike morphology, as seen before for the separation layer on top exclusively (Figure 3B). With raising THF content, the structure became less compact (Figure 3D, upper inset, 40% THF) and, as seen for $S_{81}D_{19}^{75}$, wormlike structures were again developed at the bottom surface (Figure 3D, lower inset). This got even more pronounced for a THF content of 50% (Figure 3F, lower inset). Also here, the cylindrical structures appeared further developed, with fewer branches and a higher aspect ratio. Along

with the apparent higher porosity, the overall film thickness increased as well. For 25 and 40% THF, films with around 40−45 μm were obtained whereas for ≥50% THF a thickness of 65 μm could be determined via SEM. If 60% THF were used in the casting solution, a transition in the membrane structure could be seen. Figure 3H displays an asymmetric structure again, as found for $S_{81}D_{19}^{75}$ before (Figure 2). Clearly, a compact barrier layer was formed on top of the membrane (Figure 3H, upper inset) with a thickness of 5−10 μm. The macrovoids here were not "fingerlike", instead they were "pear-shaped". This could also be attributed to the increased PDMAEMA content and the better compatibility between polymer and nonsolvent, altering the kinetics of the phase separation (20). The bottom view (Figure 3H, lower inset) presents a rather packed network of branched cylindrical structures. After casting with the highest THF content, 75%, the overall membrane morphology was comparable (Figure 3J). Here, the "pear-shaped" appearance of the macrovoids was even more pronounced. Also, different layers of macrovoids were present, scarcely one example penetrating from the separation layer to the bottom was found. The structure within the top layer did not show any difference (Figure 3J, upper inset), whereas the branching tendency within the bottom surface increased (Figure 3J, lower inset).

Regardless of the polymer, the variation of the solvent mixture composition has two consequences: with increasing THF content, the compatibility between solvent and nonsolvent slightly decreases whereas the viscosity decreases considerably; both, thermodynamic and kinetic, effects should lead to faster overall phase separation. However, if compared, the solvent composition of the casting solution did not have a drastic effect on the obtained membrane structures for $S_{81}D_{19}^{75}$. Depending on the THF content, slight variations in the thickness of the separation layer on top of the membranes were observed. Furthermore, at certain compositions a more controlled phase separation of the block copolymer was promoted in close proximity to the glass substrate, resulting in cylindrical structures. This could be explained by the composition gradient throughout the polymer film, which develops following immersion of the "proto membrane" into the water bath leading to a delayed precipitation so that defined block copolymer aggregation could take place before. In contrast, for $S_{68}D_{32}^{100}$, the solvent composition played an important role. Up to 50% THF in the initial casting solution, membranes with an isotropic cross-section were obtained. First, this could be explained through the higher compatibility of the used block copolymer with the coagulation bath caused by the higher content in hydrophilic material, PDMAEMA. Second, during the "open time", mostly THF evaporates and the DMF content increased in the as-cast polymer film. As DMF is supposed to be the better solvent for PDMAEMA this further enhances the described effect. In combination, both shifted the system away from rapid demixing and resulted in a more compact membrane structure. If a sufficiently high THF content was used for film casting, the same "open time" caused enough solvent depletion so that upon immersion in the water bath, rapid demixing also occurred for this polymer. In this case, 60% THF have proven to be enough, as shown in Figure 3H. To our opinion, the structures obtained at the bottom surface fortify the drawn conclusions. The higher compatibility of $S_{68}D_{32}^{100}$ with water resulted in a slower precipitation and, for all solvent compositions except 25% THF, in well-defined cylindrical aggregates. At the same time, the increasing overall content of the good solvent for PS (THF) also favored the delayed precipitation as precondition for the formation of defined aggregates of the block copolymer. Up to now, no absolutely conclusive explanation could be given for the amount of branching observed for these structures. The tendency for $S_{68}D_{32}^{100}$, however, seemed to increase with the THF content, as shown in the lower insets of Figure 3D, F, H, and J. Overall, the block copolymer and its composition had a decisive influence on the porous membrane morphology resulting from the NIPS process, and for $S_{68}D_{32}^{100}$ the selective solvent properties for the two blocks could be used to change the pore structure (whereas viscosity is of less importance). The morphological features obtained at the bottom of the membranes, unfortunately, could scarcely be compared with solution-based aggregation experiments (cf. above), as the actual solvent composition at the point of immersion was hard to determine.

Influence of the "Open Time". As described earlier, asymmetric cross-section structures were desired for high-flux membranes. Hence, the solvent compositions taken for the investigation of the "open-time" were 50% THF/50% DMF in the case of $S_{81}D_{19}^{75}$ and 60% THF/40% DMF for $S_{68}D_{32}^{100}$. The casted film thickness was 200 μm in all cases. For both polymers, experiments were carried out with "open times" between 0 s and 10 min. To avoid any misinterpretation, we clearly state that 0 s corresponded to an immediate immersion of the as-cast film into the water bath. Nevertheless, a delay of a few seconds due to the removal of the doctor blade, and of course, the casting process itself, could not be avoided. First, results for both polymers are described separately and are afterward compared.

$S_{81}D_{19}^{75}$. Membranes were cast from solutions of $S_{81}D_{19}^{75}$ with "open times" of 0, 30, 60, and 90 s and 2 and 3 min. For times exceeding 90 s, no further difference in the membrane structure could be found. SEM micrographs of membrane cross-sections obtained for different "open times" are shown in Figure 4. The upper insets show an enlargement of the structure at the separation layer on top of the membranes. In one case, an on-top view onto the membrane surface in contact with air is shown in the lower inset. Figure 4A shows a cross-section obtained after 0 s. Clearly, the asymmetric nature of the membrane could be seen. The top layer (Figure 4A, inset), however, appears far more dense and does not show any pores. Obviously, the very short "open time" prevented the system from the formation of a porous top layer. Indeed, the membrane did not exhibit any measurable water flux (cf. below), hinting to a nonporous top layer. However, this will be discussed in

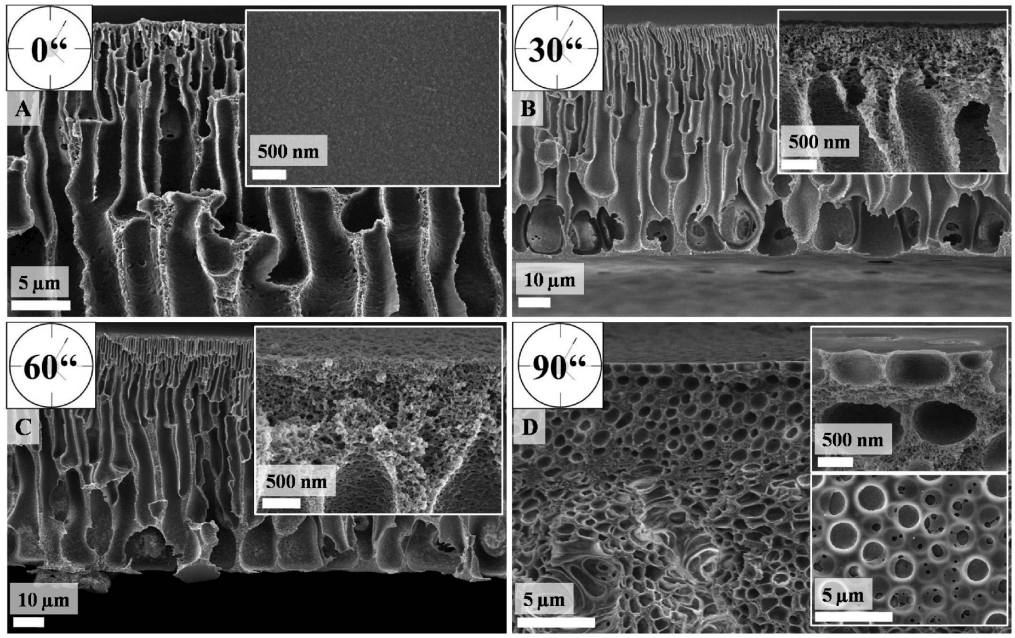

FIGURE 4. SEM micrographs for membranes from $S_{81}D_{19}^{75}$ cast from a mixture of THF (50%) and DMF (50%) after different "open times": (A) 0, (B) 30, (C) 60, and (D) 90 s; the upper insets show (A) the membrane top surface and (B, D) an enlargement of the respective separation layer; the lower inset (D) displays a top view onto the top layer.

more detail later. Beneath, "fingerlike" macrovoids were obtained, attributed again to the rapid demixing process.

After 30 s "open time", the formation of a porous top layer was already evident, as shown in Figure 4B. This separation layer exhibited a thickness of around 1 μm. After 60 s, almost no difference in the membrane structure was obtained (Figure 4C). The top layer increased slightly in thickness. This situation changed if the "open time" was increased to 90 s. Here, the membrane no longer showed an asymmetric cross-section (Figure 4D). Instead, a spongelike morphology was obtained throughout the whole film. Obviously, through the solvent evaporation during these 90 s, a too high polymer concentration was reached and phase separation occurred even before the immersion into the water bath. In the lower inset of Figure 4D an on-top view onto the membrane top layer is shown. Comparable to the cross-section, spherical holes in the range of 2−5 μm could be seen. Similar observations were made if the "open time" was increased beyond 90 s, but the macropore dimensions did not further increase with open-time.

$S_{68}D_{32}^{100}$. Membranes were cast from solutions of $S_{68}D_{32}^{100}$ with "open-times" of 0, 30, 60, and 90 s and 2, 3, and 10 min. SEM micrographs of the membranes cross-sections obtained for different "open times" are shown in Figure 5.

If the as-cast film was immersed into the coagulation bath immediately, both separation layer and the volume structure were less developed (Figure 5A). The top layer, like observed for $S_{81}D_{19}^{75}$, exhibited a thickness below 500 nm and showed no pores (Figure 5A, upper inset). Also here, no water flux could be obtained (cf. below). The macrovoids beneath were rather broad and ill-defined. At the bottom surface, interconnecting wormlike objects were observed (Figure 5A, lower inset). After 60 s, the membrane structure was as already described in the previous chapter. A compact separation layer with a thickness of around 10 μm is formed, supported from underneath by "pear-shaped" macrovoids. If longer "open times" were used, the membrane morphology changed. After 2 min, an isotropic cross section was obtained (Figure 5C), comparable to the structures obtained for 60 s and a lower THF content in the casting solution (cf. Figure 3B, D, F). A possible explanation is that the long "open time" resulted again in a depletion of the polymer film from THF, leading to phase separation occurring before the immersion step. Contrary to $S_{81}D_{19}^{75}$, where a spongelike structure with features in the region of 2−5 μm was formed, for $S_{68}D_{32}^{100}$, a densely packed spongelike structure could be seen. Again, the altered block copolymer composition played an important role. As DMF is the better solvent for PDMAEMA, its higher content improved the solubility of the block copolymer even at higher concentrations in the remaining solvent mixture, now mainly consisting of DMF. As a direct result, more defined structures could be obtained for $S_{68}D_{32}^{100}$ even for long "open times". This could also be seen in the lower inset of Figure 5C, where wormlike structures are shown at the bottom surface of the membrane. To further elucidate this statement, an as-cast polymer film was left for 10 min prior to immersion. In this particular case, all THF should have been evaporated and the "proto-membrane" should only consist of polymer and DMF. Clearly, the obtained membrane (Figure 5D) exhibits a similar structure as the one formed after 2 min. If combined with the results discussed for different solvent compositions, the tendency for the formation of branches for the cylindrical structures at the bottom surface of the membranes seems to increase with the "open time". For 10 min, scarcely single, unconnected cylinders can be seen (Figure 5D, lower inset).

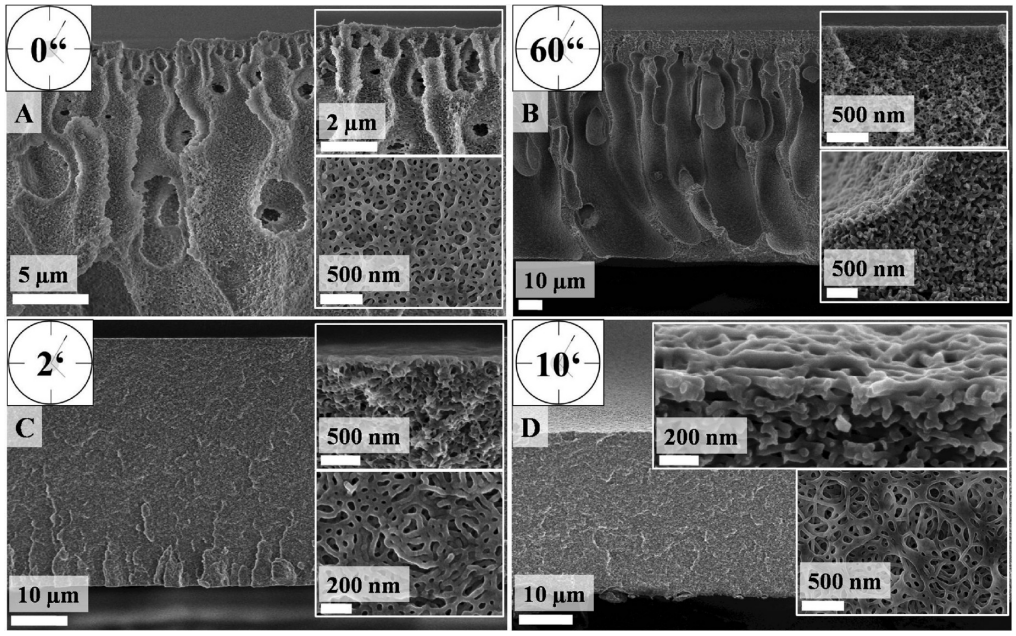

FIGURE 5. SEM micrographs for membranes from $S_{68}D_{32}^{100}$ cast from a mixture of THF (60%) and DMF (40%) after different “open-times”: (A) 0 s, (B) 60 s, (C) 2 min, and (D) 10 min; the upper insets show an enlargement of the respective separation layer, the lower insets display the morphology obtained at the bottom of the membrane.

Comparison of Both Block Copolymers. An increase in “open time” over a certain critical value resulted in macrophase separation taking place prior to the immersion into the coagulation bath for both block copolymers investigated. This critical value was determined through both the content in hydrophilic material, PDMAEMA, and THF. Because of the high volatility of THF, the amount of THF in the casting solution determined the actual polymer concentration at comparable “open times”. For the polymer with the lower content of DMAEMA, $S_{81}D_{19}^{75}$, the critical value was reached after 90 s. Here, the polymer already precipitated in the as-cast film, as could be observed by the transition to a turbid film. After immersion in the coagulation bath, an isotropic cross-section with a comblike morphology had formed. The longer PDMAEMA block of $S_{68}D_{32}^{100}$ yielded a higher compatibility with the water bath and also kept the block copolymer soluble at higher concentrations. Thus, even for an “open time” of 10 min, more developed microphase separated porous features could be obtained as displayed in Figure 5D.

Influence of Casted Film Thickness. After the discussion of the role of the solvent composition of the casting solution and the “open time”, the next important parameter was the step height used for film casting. A thicker film contains more solvent and, because of mass transfer over the same area, should slower deplete with respect to the THF content. The influence of the casted film thickness was investigated for $S_{81}D_{19}^{75}$. Films with 50, 100, 150, and 200 μm thickness were cast like described before. The solvent composition was 50% THF and 50% DMF. The “open time” was kept at 60 s. The resulting SEM micrographs are shown in Figure 6. Note that only cross-sections for 50, 100, and 150 μm initial film thicknesses are shown here; for 200 μm, the reader is referred to Figures 3C or 4C.

For a film thickness of 50 μm, a spongelike membrane structure was obtained (Figure 6A), very similar to the one from a 200 μm film after an “open time” of 90 s (Figure 4D). Both in the volume and on the surface, structural features in the range of 2−5 μm and with a spherical shape could be seen. We suppose that this could be explained in a similar manner like for the “open time”. For a thinner as-cast film, the critical polymer concentration was reached after a shorter time period, 60 s in this case. This is again due to the evaporation of the THF, the better solvent for the majority block, PS. For a 100 μm step height, a comparable membrane structure could be observed (Figure 6B). However, throughout the cross-section, some locations were found where the cell structure seems to be disturbed. This could already be an indication for the beginning of the macrovoid formation. Apart from that, shape and size of the obtained structures matched. The transition toward an asymmetric membrane morphology was reached if films with an initial thickness of 150 μm were cast (Figure 6C). “Fingerlike” macrovoids were obtained beneath a dense skin layer with a thickness of around 5 μm. However, the structure was still not as defined as for films with 200 μm casting thickness, the macrovoids did not penetrate the whole supporting volume, and another compact layer was formed on the bottom of the membrane.

Overall, the results of variation of casted film thickness and varied “open time” could consistently be discussed based on evaporation of THF from the solvent mixture, controlled by the mass transfer to the film surface, with the same influences on the transition from anisotropic to isotropic porous cross-section morphologies. It should also be possible to favor the formation of controlled microphase separated morphologies via casted film thickness (or its

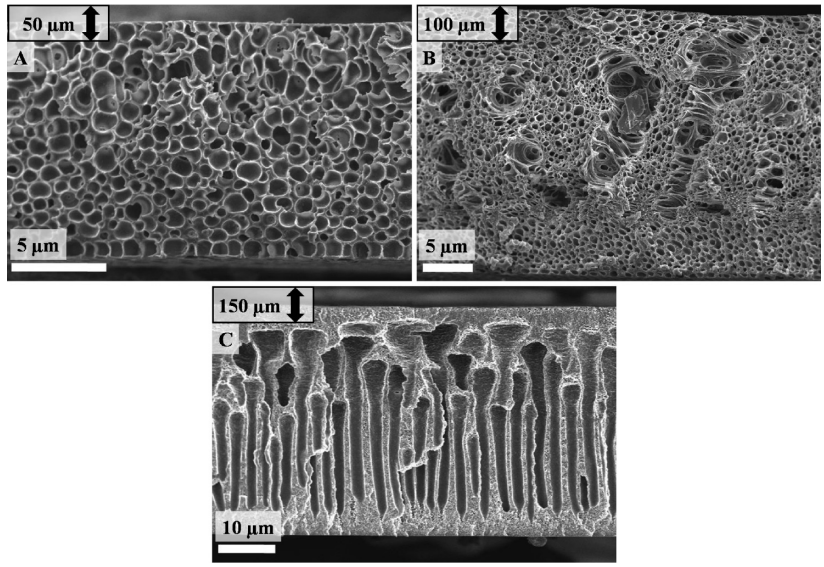

FIGURE 6. SEM micrographs for membranes from $S_{81}D_{19}^{75}$ cast from a mixture of THF (50%) and DMF (50%) with 60 s "open time" for different film thicknesses: (A) 50, (B) 100, and (C) 150 μm.

combination with "open time") if the respective copolymer/solvent system will allow this (cf. above).

Tunable Water Flux. After varying the preparation parameters, the water flux through the obtained membranes was determined. First, the influence of the casting solvent mixture composition and "open-time" will be discussed. Afterward, the double stimuli-responsive character of those structures will be highlighted using two representative examples: membranes from both $S_{81}D_{19}^{75}$ and $S_{68}D_{32}^{100}$ cast from a mixture of 60% THF and 40% DMF with 200 μm film thickness and 60 s "open time". Water flux values obtained with deionized water (pH 6) at 25 °C for both polymers and different preparation conditions are summarized in Table 1.

Table 1 shows the water flux values for different compositions of the solvent mixture for film casting. In the case of $S_{81}D_{19}^{75}$, high flux values were obtained except for the lowest THF content, 25%. Although this was not visible in the SEM micrographs, the skin layer for this membrane seemed to be less porous. For higher THF contents larger flux values were measured. As observed in Figure 3 concerning the morphological features, also the water flux showed no distinct tendency for THF contents ranging from 40 to 75%. The membranes cast from solutions containing 40 and 60% THF exhibited the highest flux values with around 4000. For 50 and 75% THF, permeabilities of 2500 and 1400, respectively, were determined.

For the diblock copolymer with the longer PDMAEMA block, $S_{68}D_{32}^{100}$, low flux values were measured for THF contents in the solvent mixture of 25, 40, and 50%. This could be explained by the compact, isotropic cross-section of these membranes (cf. Figure 3B, D, and F). The membrane cast from 60% THF and 40% DMF, exhibiting the desired asymmetric structure, showed a drastically increased flux with a value of 2100. If the THF content was increased further to 75%, the flux decreased again although the membrane cross section still was anisotropic in nature. A possible explanation is the earlier discussed transition from "fingerlike" toward "pear-shaped" macrovoids. Furthermore, these structural features did not penetrate the whole membrane any more, resulting in a reduced permeability.

Table 1 also summarizes the results for different "open times". For $S_{81}D_{19}^{75}$, no flux could be measured if this period is either too short or too long. For 0 s, the skin layer did not exhibit any porosity (Figure 4A), for 90 s phase separation already started before the immersion into the water bath, leading to a spongelike cross section. As mentioned earlier, longer "open times" than 90 s did not lead to any significant change in the membrane morphology. Surprisingly, for 30 s "open time", the highest water flux was measured.

Also for $S_{68}D_{32}^{100}$, no water flux was observed for 0 s "open time". Obviously, also here a certain evaporation of THF was necessary for the formation of pores in the top skin layer. For times exceeding 60 s, spongelike isotropic membrane cross-sections were obtained again, as discussed in Figure 5. Comparable to the structures obtained for solvent mixtures with 50% THF or less, these exhibited a rather low water flux around 100, attributed to the densely packed membrane structure. This has been verified for "open times" up to even 10 min.

Next, the surrounding conditions were varied to trigger both stimuli of the "smart" PDMAEMA, pH, and temperature. To reach a new equilibrium state under flow-through conditions, each change in pH was performed over a time span of 2 h. The waiting time in between two temperatures was 1 h. Measurements were performed for two representative membranes, prepared from solutions of 60 THF and 40% DMF for both polymers. The results are shown in Figure 7.

Figure 7A displays the water flux values obtained for $S_{81}D_{19}^{75}$ at different pH- and temperature conditions. At pH 2, almost no flux was measured because of the full protonation and hence swollen state of the PDMAEMA chains. Upon heating above the previously determined

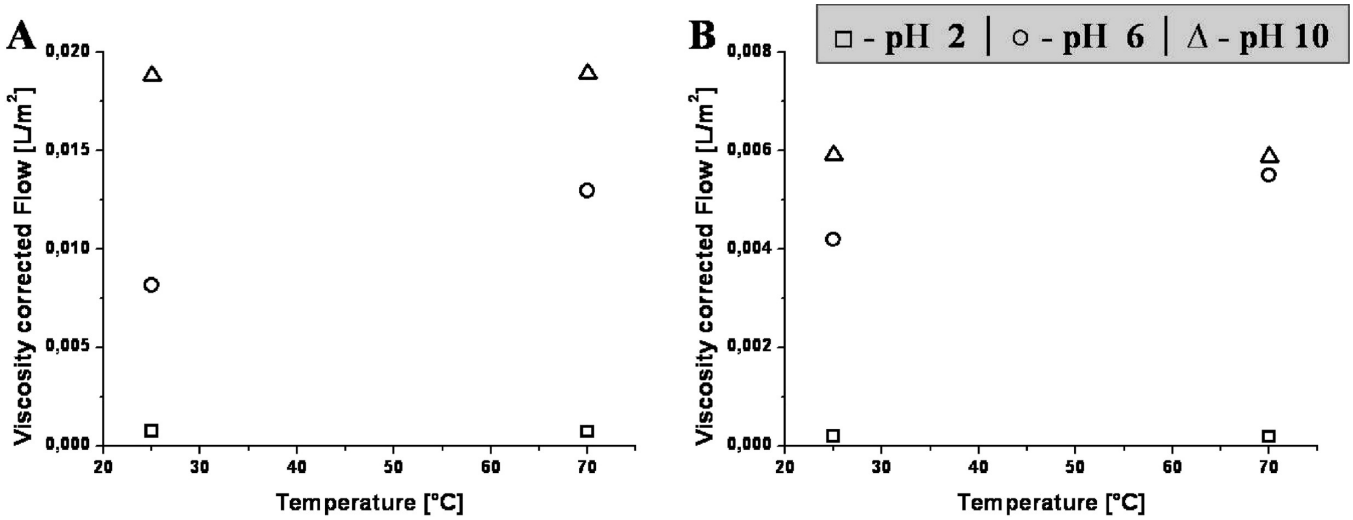

FIGURE 7. pH- and temperature-dependent water flux (multiplied with viscocity for the respective temperatures) for (A) $S_{81}D_{19}^{75}$ and (B) $S_{68}D_{32}^{100}$ membranes, prepared from solutions of 60% THF and 40% DMF; open squares indicate measurements performed at pH 2 (□), open spheres pH 6 (○), and open triangles pH 10 (Δ).

cloud point of around 65 °C for membranes prepared from this polymer (24), no increase in flux could be seen. At pH 6, the PDMAEMA chains were less protonated ($pK_a \approx 7.78$ (15)) and less extended, and a considerably higher water flux was obtained. Raising the temperature to 70 °C further increased the water flow. Here, the LCST is applicable and at the cloud point the polymer chains collapse. Through a change to pH 10 yet another gain in flux could be achieved. Under these conditions, the PDMAEMA chains were completely uncharged. Surprisingly, upon heating, no flux increase could be seen, indicating a complete collapse of the polymer chains even at room temperature.

Figure 7B summarizes the results obtained for a membrane from $S_{68}D_{32}^{100}$, prepared using the same conditions. Here, the overall flux values were lower, confirming the results presented in Table 1A. This was attributed to a more densely packed skin layer obtained for membranes of this polymer, as already discussed according to Figure 3. At pH 2, again, the hydrophilic membrane material was completely swollen, almost no flux was measured, and no gain in flux could be seen upon heating. An immense increase in terms of water flux was obtained at pH 6, almost by a factor of 20. Subsequent heating to 70 °C, like for $S_{81}D_{19}^{75}$, caused a collapse in the temperature-sensitive PDMAEMA chains, which were less protonated under these conditions. At pH 10, the largest values could be measured, and again, heating to 70 °C resulted in no further increase.

If both polymers were compared, the content of "smart" material indeed seemed to have an influence. In the case of $S_{81}D_{19}^{75}$, a change in pH from 2 to 6 induced a 10-fold water flux increase, whereas for $S_{68}D_{32}^{100}$, a factor of 20 could be seen. Further pH increase to a value of 10 resulted in a comparable change, a factor of 2 for $S_{81}D_{19}^{75}$ and a factor of 1.5 for $S_{68}D_{32}^{100}$. Same accounted for the situation upon triggering the LCST at pH 6. Here, the flux rises by a factor of 1.5 ($S_{81}D_{19}^{75}$) and 1.3 ($S_{68}D_{32}^{100}$). Obviously, the higher content of PDMAEMA leads to a higher degree of swelling of the whole membrane at low pH or, more precise, it facilitated a more pronounced deswelling upon a change to pH 6. It remains a rather puzzling question why no flux increase could be detected for both membranes upon heating at pH 10. Membranes with comparable structure, casting conditions, and flux values were shown earlier to exhibit a certain LCST behavior even under these conditions (24).

CONCLUSIONS

We successfully prepared asymmetric membranes via the NIPS process from solutions of two amphiphilic block copolymers, $S_{81}D_{19}^{75}$ and $S_{68}D_{32}^{100}$ in mixtures of DMF and THF. Through a systematic variation of the casting conditions for both polymers, e.g., the used solvent mixture, the "open time", or the casted film thickness we were able to point out crucial parameters which determine the obtained membrane morphologies. These results have to be interpreted with a certain caution, as the investigated systems are rather complex and combine the aspects of at least two different ternary phase diagrams, one for each block copolymer compartment and based on the assumption that THF and DMF mix ideally. Nevertheless, this work alludes to general tendencies and principles for morphological transitions in amphiphilic membrane systems. Moreover, the effect of a higher content in hydrophilic material for $S_{68}D_{32}^{100}$ was demonstrated, leading to an improved compatibility with the nonsolvent bath and, hence, slower precipitation and further developed structural features. Thus, conditions could be identified where ordered microphase separated porous morphologies were observed in parts of the membrane cross-section. Both polymers were shown to form self-supporting membrane systems that are able to react onto two different external stimuli in terms of water flux, pH, and temperature.

Acknowledgment. The authors thank Benjamin Gossler for the SEM measurements and Sabine Wunder, Christina

Löffler, and Robin Pettau for SEC measurements (all University of Bayreuth). Claudia Schenk, Marcel Gawenda, and Dr. Heru Susanto are acknowledged for their help during the stay of F.S. at University Duisburg-Essen. Funding was received from the VolkswagenStiftung within the framework "Complex Materials".

REFERENCES AND NOTES

(1) Baker, R. *Membrane Technology and Applications*; Wiley: Chichester, U.K., 2004.
(2) Yoo, S. H.; Kim, J. H.; Jho, J. Y.; Won, J.; Kang, Y. S. *J. Membr. Sci.* **2004**, *236*, 203–207.
(3) Ulbricht, M. *Polymer* **2006**, *47*, 2217–2262.
(4) Mehta, A.; Zydney, A. L. *J. Membr. Sci.* **2005**, *249*, 245–249.
(5) Abetz, V., Simon, P. F. W. *Phase Behavior and Morphologies of Block Copolymers*; Springer-Verlag: Berlin, 2005; Vol. 189, pp 125−212.
(6) Klok, H.-A.; Lecommandoux, S. *Adv. Mater.* **2001**, *13*, 1217–1229.
(7) Schacher, F.; Müllner, M.; Schmalz, H.; Müller, A. H. E. *Macromol. Chem. Phys.* **2009**, *210*, 256–262.
(8) Walther, A.; Millard, P.-E.; Goldmann, A. S.; Lovestead, T. M.; Schacher, F.; Barner-Kowollik, C.; Müller, A. H. E. *Macromolecules* **2008**, *41*, 8608–8619.
(9) Breiner, U.; Krappe, U.; Abetz, V.; Stadler, R. *Macromol. Chem. Phys.* **1997**, *198*, 1051.
(10) Hückstädt, H.; Göpfert, A.; Abetz, V. *Polymer* **2000**, *41*, 9089–9094.
(11) Walther, A.; Andre, X.; Drechsler, M.; Abetz, V.; Müller, A. H. E. *J. Am. Chem. Soc.* **2007**, *129*, 6187–6198.
(12) Sperschneider, A.; Schacher, F.; Gawenda, M.; Tsarkova, L.; Müller, A. H. E.; Ulbricht, M.; Krausch, G.; Köhler, J. *Small* **2007**, *3*, 1056–1063.
(13) Erhardt, R.; Boker, A.; Zettl, H.; Kaya, H.; Pyckhout-Hintzen, W.; Krausch, G.; Abetz, V.; Müller, A. H. E. *Macromolecules* **2001**, *34*, 1069–1075.
(14) Plamper, F. A.; Becker, H.; Lanzendörfer, M.; Patel, M.; Wittemann, A.; Ballauff, M.; Müller, A. H. E. *Macromol. Chem. Phys.* **2005**, *206*, 1813.
(15) Plamper, F.; Ruppel, M.; Schmalz, A.; Borisov, O.; Ballauff, M.; Müller, A. H. E. *Macromolecules* **2007**, *40*, 8361–8366.
(16) Plamper, F.; Walther, A.; Müller, A. H. E.; Ballauff, M. *Nano Lett.* **2007**, *7*, 167–171.
(17) Yang, S. Y.; Ryu, I.; Kim, H. Y.; Jang, S. K.; Russell, T. P. *Adv. Mater.* **2006**, *18*, 709–712.
(18) Phillip, W. A.; Rzayev, J.; Hillmyer, M. A.; Cussler, E. L. *J. Membr. Sci.* **2006**, *286*, 144–152.
(19) Nunes, S. P.; Peinemann, K. V., *Membrane Technology*, 2nd ed.; Wiley-VCH: Weinheim, Germany, 2006.
(20) van de Witte, P.; Dijkstra, P. J.; van den Berg, J. W. A.; Feijen, J. *J. Membr. Sci.* **1996**, *117*, 1–31.
(21) Peinemann, K. V.; Abetz, V.; Simon, P. F. W. *Nature mat.* **2007**, *6*, 992–996.
(22) Su, Y.-L.; Li, C. *J. Membr. Sci.* **2007**, *305*, 271–278.
(23) Ying, L.; Kang, E. T.; Neoh, K. G.; Kato, K.; Iwata, H. *J. Membr. Sci.* **2004**, *243*, 253–262.
(24) Schacher, F.; Ulbricht, M.; Müller, A. H. E. *Adv. Funct. Mater.* **2009**, *19*, 1040–1045.
(25) Freyss, D.; Rempp, P.; Benoît, H. *Polym. Lett.* **1964**, *2*, 217.
(26) Quirk, R. P.; Yoo, T.; Lee, Y.; Kim, J.; Lee, B. *Adv. Polym. Sci.* **2000**, *153*, 67–106.
(27) Brandrup, J.; Immergut, E. H.; Grulke, E. A., *Polymer Handbook*, 4th ed.; John Wiley & Sons: New York, 1999.
(28) Wienk, I. M.; Boom, R. M.; Beerlage, M. A. M.; Bulte, A. M. W.; Smolders, C. A.; Strathmann, H. *J. Membr. Sci.* **1996**, *113*, 361–371.

AM900175U